DEFORMABLE ADAPTIVE WALL TEST SECTION FOR THREE-DIMENSIONAL WIND TUNNEL TESTING

ICAS-84-2.1.2

A. Heddergott and E. Wedemeyer

Deutsche Forschungs- und Versuchsanstalt für Luft- und Raumfahrt e.V.
Institut für Experimentelle Strömungsmechanik, 3400 Göttingen (FRG)

Abstract

To realize three-dimensional adaptive wind tunnel walls a test section was constructed from a thick walled rubber tube. The new test section with a length of 240 cm and a circular cross section of 80cmØ is installed in the high speed wind tunnel of the DFVLR Göttingen. The cylindrical walls of the test section can be adapted to interference free boundary conditions by a set of 64 jacks which are driven by stepping motors. The measurement and evaluation of wall pressures, the computation of the interference free wall contour and the wall adaptation by the 64 jacks are computer controlled and performed automatically. First model tests have demonstrated the achievement of interference free flow.

Nomenclature

A	total wing area
A_b	body base area
A_T	test section area
c	mean aerodynamic chord
C_D	drag coefficient
C_{Db}	base drag coefficient
C_{Df}	forebody drag coefficient
C_L	lift coefficient
C_m	pitching moment coefficient
c_p	pressure coefficient
D	body diameter
D_T	test section diameter
l	length of body
L	test section length
Ma	Mach number
Re	Reynolds number
U_∞	free stream velocity
u, v	longitudinal, normal component of perturbation velocity
α	angle of attack
β	Prandtl factor = $\sqrt{1-Ma^2}$
η	wall displacement
ϕ	flow potential
(x, r, θ)	polar coordinate system

Subscripts

i, e	internal, external

1. Introduction

The need for interference free wind tunnel data in the high subsonic Mach number range has in recent years inspired the construction of wind tunnel test sections with "adaptive walls", i.e., walls that can be adapted to the streamlines of unconfined flow. In conjunction with such test sections computer codes were developed for the calculation of the adapted wall contours. The principle of adaptive or "selfstreamlining" walls was first described in publications by Sears[1] and Ferri and Baronti[2].

Streamlining the walls can be achieved either by deflection of flexible plates which form the test section walls or by wall ventilation. The latter concept can be realized by deviding the outer wall surface into a number of separated compartments so that the airstream through each compartment can be controlled by variation of the back pressure. A method which is applied at the AEDC[3] uses variable porosity of the walls with constant pressure in the plenum chamber.

An advantage of the wall ventilation methods is the capability of porous walls to absorb shock waves. On the other hand there are disadvantages due to the fact that the flow near perforated walls is quite inhomogeneous so that measurement of flow angle and static pressure cannot be performed at or near the wall. These data, which are required for the wall adaptation procedure, must then be measured inside the flow which in turn creates great difficulties.

The concept of flexible solid plates for the wall adaptation was realized mainly for two dimensional flows, especially for the testing of wing sections [4, 5, 6, 7, 8]. A remarkable exception is the three-dimensional adaptive test section at the Technical University Berlin[9] with an octagonal test section constructed from eight flexible plates and flexible "scales" between the plates.

The concept introduced in this paper uses a thick walled rubber tube for the adaptive test section. The cylindrical tube can be deformed by a set of 64 motor-driven jacks to any desired wall contour. The construction of the tube with a very smooth inner surface as well as the drilling of pressure holes into the wall provided no difficulties. The new test section was designed so that it could be installed in the existing DFVLR high speed wind tunnel at Göttingen (HWG). The HWG, which is described in Ref. 11, is a vacuum storage blowdown tunnel with an open jet

test section of $0.75 \times 0.75 m^2$ for subsonic flow and a supersonic test section with an adjustable nozzle. In its new mode of operation the square nozzle and contraction section are replaced by the rubber tube test section and a new nozzle that connects the cylindrical test section with the rectangular settling chamber.

A detailed description of the rubber tube test section is given in Section 2. Section 3 presents a method for the computation of the three-dimensional adapted wall contour. Finally, in Section 4, first results of model tests are presented and compared with interference free reference data.

2. Description of the rubber tube test section

For two-dimensional flows past wing sections etc. wall adaption has been achieved by use of flexible plates for the upper und lower test section walls. For general three-dimensional flows the walls must be three-dimensionally deformable, i.e. flexible and strechable, in order to be adjustable to the streamlines of the unconfined flow.

To realize three-dimensional adaptive walls the test section was constructed from a thick walled rubber tube. The new test section with a length of 240 cm and a circular cross section of 80 cm diameter was installed in the existing blowdown wind tunnel of the DFVLR Göttingen. Fig. 1 and 2 show schematic drawings of the DFVLR blowdown tunnel and the new test section. A photograph of the test section before installation is shown in Fig. 3.

A circular cross section was chosen for the rubber tube as it was easy to manufacture and gives most uniform load distribution on the supporting jacks.

The rubber tube is flanged at one end onto the circular nozzle. The other (free) end extends through the test chamber to the bell-shaped collector. The tube is supported and can be deformed by a set of 64 jacks which are connected to a rigid frame around the test section. The jacks are driven by stepping motors. At each of 8 cross sections 8 jacks are mounted over the circumference with equal angular distances between two adjacent jacks. The hinged connection of the jacks allows for small lateral displacement. Each jack acts via four support points on the rubber wall so that the deforming force is more evenly distributed over the surface. The supports are vulcanized into the rubber wall. The small distances between adjacent support points and a relatively large wall thickness of 6 cm assure that the wall is sufficiently stiff and that it remains smooth - i.e. free from waviness - after deformation.

The holes for pressure measurements are located at 1/4 and 3/4 position between the support points in longitudinal direction and 1/2 position between the supports in circumferential direction (Fig. 2). This has been calculated as position of minimum error due to wall waviness effects.

Wall pressures and displacement are measured at the 64 positions of the jacks. In addition to the recordings of the stepping motors 64 potentiometers are used for the measurement of the wall displacement.

The measurement of the wall data, the wall adaption, and the model testing is performed fully automatically.

PSI pressure transducer and acquisition system is used for pressure distributions on the test section walls as well as for wind tunnel models. The system allows up to 14000 pressure recordings per second with an accuracy of about 0.5×10^{-3} bar (0.725×10^{-2} psi).

At the wind tunnel a micro-computer PDP 11/23 PLUS, for data reduction and control of the wall adaptation and test procedure and a graphic-terminal VT 100 RG are available. The final evaluation of test results, storage of data and the computation of wall contours are performed at the central computer. Fig. 4 shows a control diagram of the test section.

3. Wall adaptation scheme

The principle of wall adaptation, as described by Sears[1] requires the measurement of two independent flow variables at the wall, for example normal (v) and tangential (u) velocity components. An equivalent pair of flow variables are wall pressure (p) and wall displacement (η).

For the rubber wall test section, the wall pressure is measured in a first tunnel run. The measured pressures and the initial wall displacement (which can but must not be zero) are recorded and used as input for the calculation of the adapted wall contour.

For a given wall contour a fictitious "external flow" is defined (Fig. 5) as a potential flow, which is tangential to the wall contour and passes into undisturbed parallel flow at infinity.

The external flow can be computed on the basis of potential flow theory. The computed external flow is, in general, not a physical continuation of the internal flow unless the wall pressure is continuous i.e. the measured pressure $p_{(i)}$ at the inside of the wall agrees with the computed external wall pressure $p_{(e)}$ at every point on the wall surface. The mathematical problem of wall adaptation consists of finding a wall contour for which the pressure is continuous across the wall i.e.

$p_{(i)} = p_{(e)}$. Usually this problem is solved iteratively: The wall is displaced so as to decrease the pressure jump $(p_{(i)}-p_{(e)})$. For the displaced wall a new pressure distribution $p_{(i)}$ is measured and compared with the new theoretical distributions of $p_{(e)}$ etc.

Under certain conditions the wall adaptation can be achieved within one iteration step. A one step method used for the rubber wall test section is discribed in section 3.1.

3.1 One-step method of wall adaptation

The method of wall adaptation described here is based on the assumption that the flow is subsonic near the test section walls and that the wall deflections are sufficiently small so that flow disturbances due to these wall deflections can be described by the linearized potential equation. Under the above assumption the flow induced by the wall deflections can be superimposed on the flow induced by the model.

Then, after wall deflection, the resulting flow variables on the inside of the wall must be equal to the flow variables on the outside. This condition leads to a set of linear equations for the wall deflection. In cases where supersonic pockets extend up to the test section wall the proposition of linearized flow theory is certainly incorrect and a more elaborate iterative method becomes necessary for the adaptation of the wall.

The one step method, whenever it is applicable, is preferable as it computes the adapted wall contour in one iteration step and so saves tunnel running time.

A cylindrical coordinate system (x, r, θ) is used with velocity components (u, v, w) respectively. The wall displacement is denoted by $\eta(x,\theta)$ i.e. the displaced wall has a distance from the centre line which is $R = R_o+\eta(x,\theta)$ (Fig. 5). The initial wall displacement is denoted by $\eta_o(x,\theta)$. η_o can e.g. be identically zero. It is, however, useful to chose for η_o the wall setting of the previous measurement at neighbouring Mach number or angle of incidence.

For the initial wall setting η_o the interior flow about the model can be described (at least in the wall region) by a perturbation potential $\Phi_o(x,r,\theta)$. Φ_o is unknown but the velocity components at the wall $u_o = (\partial\Phi_o/\partial x)_R$ and $v_o = (\partial\Phi_o/\partial r)_R$ are known by measuring the wall pressure $(\Delta p_o = -\rho U_\infty u_o)$ and the wall displacement $(v_o = U_\infty\, d\eta_o/dx)$.

An additional wall displacement $\Delta\eta = \eta_1-\eta_o$ generates an additional perturbation potential $\varphi_{(i)}$. The perturbation potential for the outer flow may be denoted by $\varphi_{(e)}$. $\varphi_{(i)}$ and $\varphi_{(e)}$ are solutions of the linearized potential equation:

$$\beta^2\varphi_{xx} + \varphi_{rr} + \frac{1}{r}\varphi_r + \frac{1}{r^2}\varphi_{\theta\theta} = 0$$

Taking advantage of the cylindrical geometry of the test section, we can expand $\varphi_{(i)}$ and $\varphi_{(e)}$ in a Fourier series. The total perturbation potential for the internal flow can then be written:

$$\Phi_{(i)} = \Phi_0+U_\infty\sum_{n,k} a_{n,k}I_n(\beta kr)e^{i(n\theta+kx)}. \qquad (1)$$

For the fictitious external flow we assume a perturbation potential:

$$\Phi_{(e)} = U_\infty\sum_{n,k} b_{n,k}K_n(\beta kr)e^{i(n\theta+kx)} \qquad (2)$$

I_n and K_n are adjoint Bessel functions. Since the perturbation due to the wall displacement must have no singularities, only the I_n can be used for the internal flow (Equ. 1) and for the external flow only the K_n can be used as only the K_n are bounded for $r \to \infty$.

The coefficients $a_{n,k}$ and $b_{n,k}$ are now determined by the following conditions:

$v_{(i)} = v_{(e)}$ and $u_{(i)} = u_{(e)}$ with

$$v_{(i)} = \left(\frac{\partial\Phi_{(i)}}{\partial r}\right)_R ; \quad v_{(e)} = \left(\frac{\partial\Phi_{(e)}}{\partial r}\right)_R ;$$

$$u_{(i)} = \left(\frac{\partial\Phi_{(i)}}{\partial x}\right)_R ; \quad u_{(e)} = \left(\frac{\partial\Phi_{(e)}}{\partial x}\right)_R .$$

With Eqs. (1) and (2) we get:

$$v_{(i)} = v_0+U_\infty\sum_{n,k} a_{n,k}I_n'(\beta kR).\beta k e^{i(n\theta+kx)} \qquad (3)$$

$$v_{(e)} = U_\infty\sum_{n,k} b_{n,k}K_n'(\beta kR).\beta k e^{i(n\theta+kx)} \qquad (4)$$

By integration of Eqs. (3) and (4) we get:

$$\eta_{1(i)} = \eta_0+\sum_{n,k}\frac{\beta}{i}a_{n,k}I_n'(\beta kR)e^{i(n\theta+kx)} \qquad (5)$$

$$\eta_{1(e)} = \sum_{n,k}\frac{\beta}{i}b_{n,k}K'_n(\beta kR)e^{i(n\theta+kx)} \qquad (6)$$

For the tangential velocity components Eqs. (1) and (2) give:

$$u_{(i)} = u_0 + U_\infty \sum_{n,k} a_{n,k} ik\, I_n(\beta kR) e^{i(n\theta+kx)} \quad (7)$$

$$u_{(e)} = U_\infty \sum_{n,k} b_{n,k} ik\, K_n(\beta kR) e^{i(n\theta+kx)} \quad (8)$$

From $\eta_{(i)} = \eta_{(e)}$ and $u_{(i)} = u_{(e)}$ we obtain with Eqs. 5 to 8:

$$\eta_0 = \sum_{n,k} \frac{\beta}{i} (b_{n,k} K_n' - a_{n,k} I_n') e^{i(n\theta+kx)} \quad (9)$$

$$\frac{u_0}{U_\infty} = \sum_{n,k} ik (b_{n,k} K_n - a_{n,k} I_n) e^{i(n\theta+kx)} \quad (10)$$

Fourier transformation of Eqs. (9) and (10), gives:

$$\frac{\beta}{i} (b_{n,k} K_n' - a_{n,k} I_n') = \frac{1}{(2\pi)^2} \iint \eta_0 e^{-i(n\theta+kx)}\, d\theta dx \quad (11)$$

$$ik (b_{n,k} K_n - a_{n,k} I_n) = \frac{1}{(2\pi)^2} \iint \frac{u_0}{U_\infty} e^{-i(n\theta+kx)} d\theta dx \quad (12)$$

Finally, Eqs. (11) and (12) can be solved for $a_{n,k}$ and $b_{n,k}$.

It is:

$$b_{n,k} = \frac{I_n' \iint \frac{u_0}{U_\infty} e^{-i(n\theta+kx)} d\theta dx}{ik(2\pi)^2 (I_n' K_n - I_n K_n')} + \frac{\frac{k}{\beta} I_n \iint \eta_0 e^{-i(n\theta+kx)} d\theta dx}{ik(2\pi)^2 (I_n' K_n - I_n K_n')} \quad (13)$$

Inserting $b_{n,k}$ into Eq. 6 gives the wall displacement $\eta_1 = \eta_{1(e)}$:

$$\eta_1 = \frac{\beta}{i} \sum b_{n,k} K_n'(\beta kR) e^{i(n\theta+kx)} dk \quad (14)$$

The computational procedure is described in detail in Ref. 10.

4. Model tests

A number of model tests have been performed in order to demonstrate the capability of the adapted test section in producing interference free data and to investigate its limitations. Table 1 shows a survey of our model tests and reference tests of other facilities. A few remarks are made about the tunnel calibration in section 4.1. The results of the model tests are discussed in section 4.2 (pressure distribution measurements) and 4.3 (force measurements).

4.1 Calibration of the empty test section

To compensate for displacement effects of the wall boundary layer, the walls must be adjusted slightly divergent. This is - in principle - easy to attain for the rubber wall test section. A computer program, similar in structure as the program for wall adaptation, was used to adapt the walls to the condition of constant undisturbed pressure. It was an unexpected experience that errors in pressure measurement due to faulty pressure holes have a striking effect on the resulting wall contour. A provisional method of averaging was used to overcome the difficulties at first. It appears, however, desirable to calibrate all pressure taps, a task which is presently pursued.

The wall adjustment that gives zero pressure coefficients for the empty test section is taken as reference and referred to as "not adapted" or "aerodynamically straight" wall.

4.2 Pressure distribution measurements on FFA calibration model

The FFA calibration model[12] used for pressure distribution tests has a blockage ratio of 3.1 % in the not adapted test section, so that large wall interference effects could be expected. Fig. 6 shows the model, which is a parabolic spindle supported by a cylindrical afterbody, in the test section. Figs. 7 to 9 give the results of pressure measurements for adapted and not adapted walls for Mach numbers from Ma = 0.6 to Ma = 0.8. For Ma = 0.85 only the data for adapted walls are shown (Fig. 10) as the not adapted test section was choked. The strong wall interference for straight walls is completely reduced after wall adaptation as shown by comparison with theoretical interference free data. Unfortunately, no interference free experimental data for comparison were available in the tested

Mach number range.

The theoretical data are based on linearized theory and may become faulty for Ma ≥ 0.8. A partial comparison with experimental data is shown in Fig. 11 where the minimum c_p-values are plotted versus Mach number. The extrapolation of the curve to Ma = 0.9 compares well with a theoretical value computed at FFA.

At the present time it is not possible to perform tests in the adaptive test section for Mach numbers larger than 0.85. It is hoped that higher Mach numbers can be achieved after calibration of the wall pressure taps.

Fig. 12 shows the - axisymmetric - wall displacement for the FFA model after the wall has been adapted. The practicability of the one-step iteration method is clearly demonstrated as the second to fourth iteration did yield no improvement.

4.3 Force measurements on two AGARD-calibration models

Force measurements were carried out on two AGARD-calibration models of different size with tunnel blockage ratios of 1 % and 3.5 %, respectively. The experimental data are compared with data of other wind tunnels[13] which are considered as interference free reference data as they were obtained in slotted or perforated test sections with very low blockage ratios.

The ralative dimensions of the AGARD-calibration model are shown in Fig. 13. Figs. 14 to 20 show the experimental results for the force coefficients C_L, C_m, C_D, and the forebody and base drag C_{Df}, C_{Db}. The agreement with interference free reference data is remarkably good even for the large model (with 3.5 % blockage ratio and 26 % wing surface to tunnel cross section area). To give an impression of the wall interferences, data for the not adapted wall are shown in the diagrams for Ma = 0.5. For large Mach numbers the not adapted test section is again choked.

In Fig. 19 drag- and forebody drag data are plotted versus Mach number. The reference data from the TWG perforated test section with 0.5 % blockage are somewhat larger than our data. It is very likely that these reference data are still influenced by wall interference effects. Also the free flight data for C_D are larger which is plausible because the effect of the sting support on the model is to reduce the drag coefficient of the wind tunnel data compared with free flight data.

The base drag data shown in Fig. 20 are again in good agreement with all reference data. The base drag in the not adapted test section for the large model is very high, an effect which can be explained by the wake induced axial pressure gradient.

5. Conclusions

The concept of the rubber tube test section for three dimensional adaptive wall wind tunnel testing proved to be very successful. First model tests have demonstrated that interference free flow can be achieved.

The measurement of wall pressures needs further attention. Apparently due to faulty pressure taps, the calibration of the test section and model tests could not be performed for Mach numbers larger than 0.9. An improvement is expected from the calibration of the individual pressure orifices.

6. References

1. Sears, W.R., "Self-correcting wind tunnels," Aeron. Journal, Vol 78, Febr.-March 1974

2. Ferri, A., Baronti, P., "A method for transonic wind tunnel corrections," AIAA Journal, Vol. 11, Jan. 1973

3. Parker Jr., R.L., Erickson Jr., J.C., "Development of a three-dimensional adaptive wall test section with perforated walls," AGARD-CP-335, May 1983

4. Chevallier, J.P., "Soufflerie transsonique a parois auto-adaptable," ONERA T.P.n° 1975-119, 1975

5. Ganzer, U., "Windkanäle mit adaptiven Wänden zur Beseitigung von Wandinterferenzen," Z. Flugwiss. Weltraumforsch. 3 (1979), Heft 2

6. Chevallier, J.P., Mignosi, A., Archambaud, J.P., Seraudie, A., "Parois adaptable à T2," Recherche Aerospatiale n° 4, 1983

7. Schairer, E.T., Mendoza, J.P., "Adaptive-wall tunnel-research at AMES research center," AGARD-CP-335, May 1982

8. Goodyer, M.J., Wolf, S.W.D.,"Development of a self-streamlining flexible walled transonic test section," AIAA Journal, Vol. 20, No. 2, Febr. 1982

9. Ganzer, U., "On the use of adaptive walls for transonic wind tunnel testing," AGARD-CP-335, May 1982

10. Müller-Wichards, D., Gülzow, V., "Ein potentialtheoretisches Näherungsverfahren zur Berechnung der Kontur einer adaptiven Meßstrecke," DFVLR-Bericht IB 262-84 R 01

11. Ludwieg, H., Hottner, T., "Hochgeschwindigkeitskanal der Aerodynamischen Versuchsanstalt Göttingen," Z. Flugwiss. 7 (1959), Heft 10

12. Berndt, S.B., "Flow properties of slotted-wall test sections," AGARD-CP-335 May 1982

13. Schneider, W., "Drei-Komponentenmessungen an den AGARD-Eichmodellen B und C im Transsonischen Windkanal der AVA," DLR-FB 66-10, Februar 1966

Ref	Symbol	Institute	Facility	Test Section				Measurements	Blockage	Reynolds	Remarks
				Size	Walls	Open [%]	Slot Depth		[%]	Number [x10^{-6}]	
12	○	DFVLR	HWG, Adapt. Test Section	Dia. 0.8 m	cylindrical	0	–	Pressure	3.1	12.9 (*)	Same model
	⬭	"	" " "	"	adapted	0	–	Distribution	3.1	12.9	
	□	FFA	Transonic Wind Tunnel	0.89 x 0.89 m^2	slotted	9.2	18.9 mm	FFA-Model	2.2	9.7	
	⬭	DFVLR	HWG, Adapt. Test Section	Dia. 0.8 m	adapted	0	–	ONERA-C5	3.67	9.7	Same model
	x	NASA-Ames	Transonic Wind Tunnel	3.35 x 3.35 m^2	slotted	5.8	–	" "	0.17	13.8	Trans. fixed
11	○	DFVLR	HWG, Adapt. Test Section	Dia. 0.8 m	cylindrical	0	–		3.5	2.5 - 4.5 (**)	Same Model
	0	"	" " "	"	adapted	0	–	6-Comp. Force	3.5	2.5 - 4.5	
	⬭	"	" " "	"	"	0	–	AGARD - Cal.	1.0	1.4 - 2.4	
	□	"	TWG (Trans. Wind Tunnel)	1.0 x 1.0 m^2	4 perforated	6	–	Model B	0.5	1.6 - 2.6	
	△	AEDC	Transonic Model Tunnel	0.31 x 0.31 m^2	"	6	–		2.5	1.6 - 2.0	
	◇	"	PTW Transonic Circuit	4.88 x 4.88 m^2	"	6	–		0.01	0.7 - 1.2	
	▽	"	" " "	"	"	6	–		1.15	8.5 - 1.2	
	x	NACA	Free Flight							1.0 - 2.7	

(*) based on L
(**) based on l_μ

Table 1 General data on models and facilities

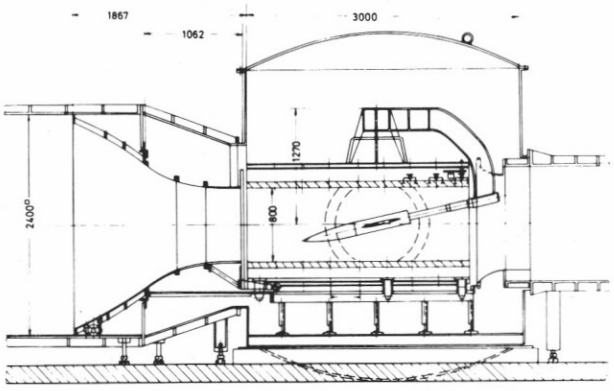

Fig. 1 High speed wind tunnel with deformable adaptive test section

Mach number range	Ma=0.4÷1.0
Maximum operating time	t =45 sec
Test section area	A_T=0.5026 m²
Contraction ratio	C =11.5

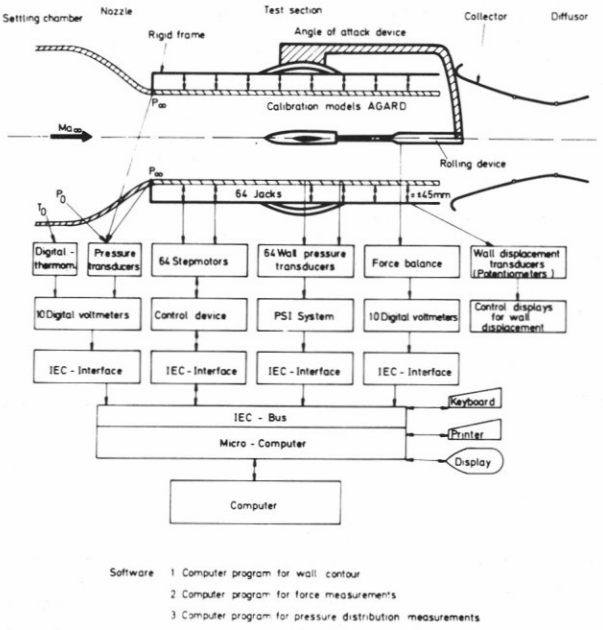

Fig. 4 Control diagram of deformable adaptive test section (DAT)

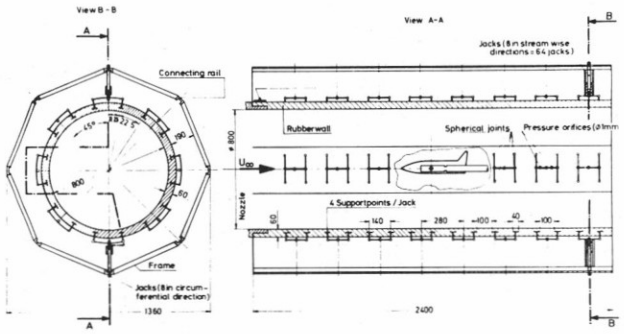

Fig. 2 Adaptive rubber tube test section for 0.8 m high speed wind tunnel at DFVLR Göttingen

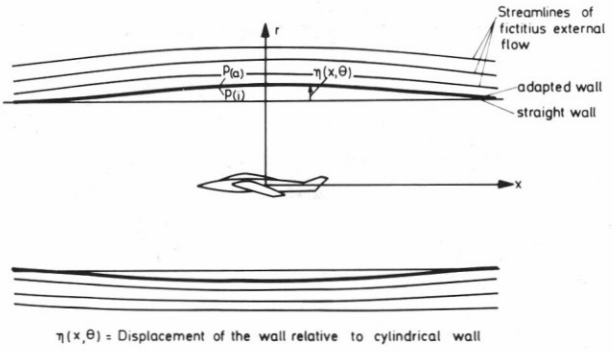

Fig. 5 The principle of adaptive walls

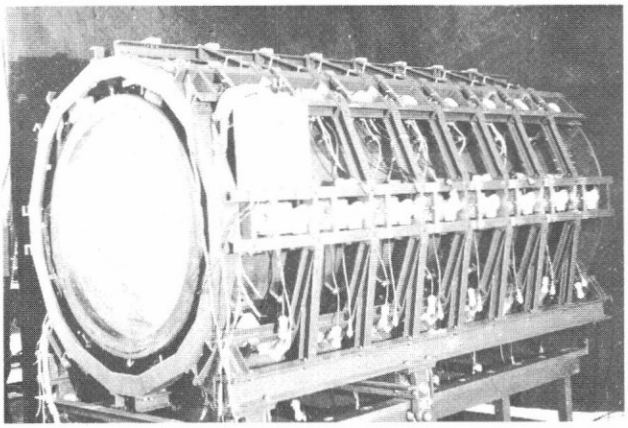

Fig. 3 Photograph of the adaptive rubber tube test section

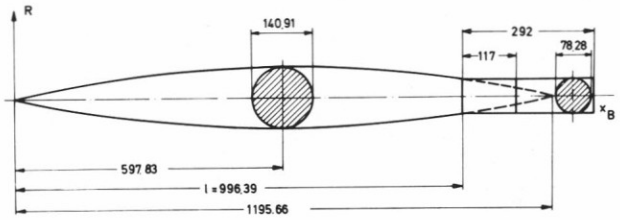

Fig. 6 FFA calibration model (parabolic spindle) for pressure measurements (Blockage ratio = 3.1 %)

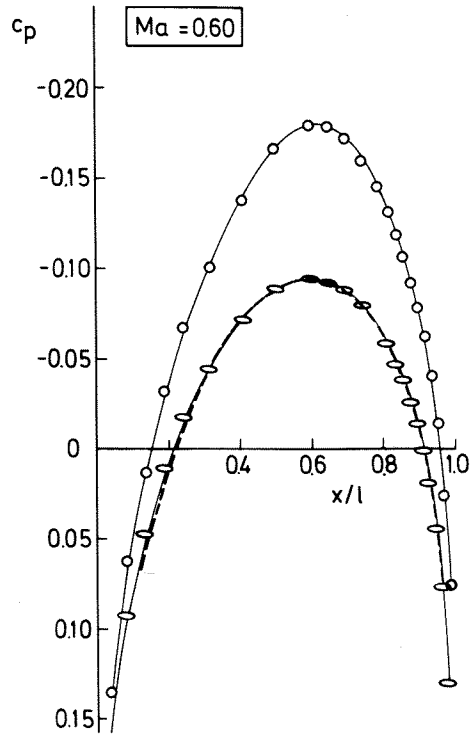

Fig. 7 Pressure distribution for FFA-model
o not adapted ⬭ adapted ---theor.

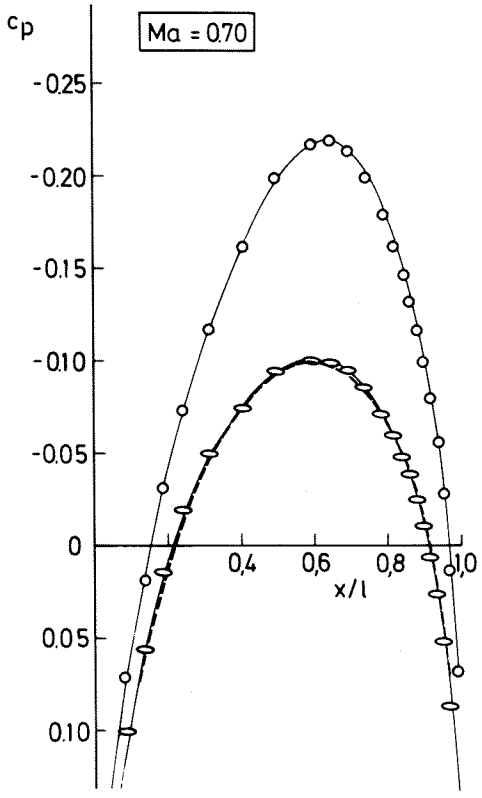

Fig. 8 Pressure distribution for FFA-model
o not adapted ⬭ adapted---theor.

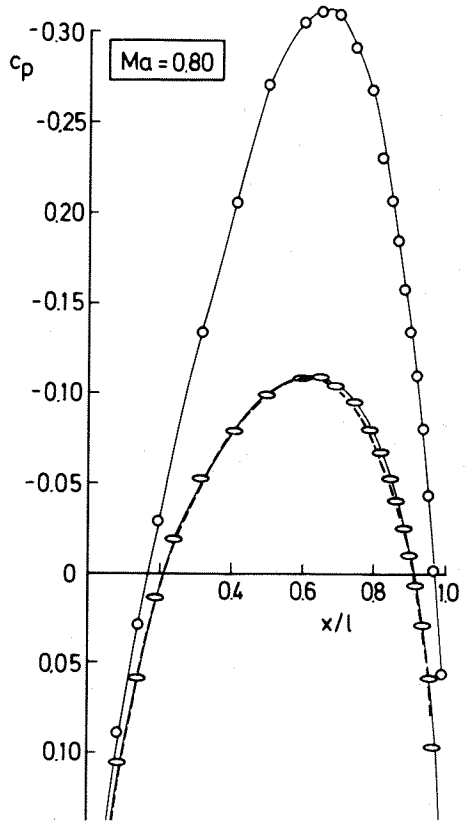

Fig. 9 Pressure distribution for FFA-model
o not adapted ⬭ adapted---theor.

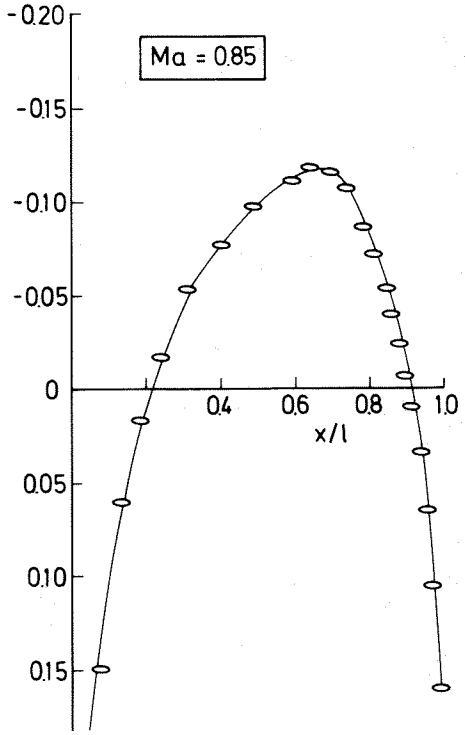

Fig. 10 Pressure distribution for FFA-model
⬭ adapted

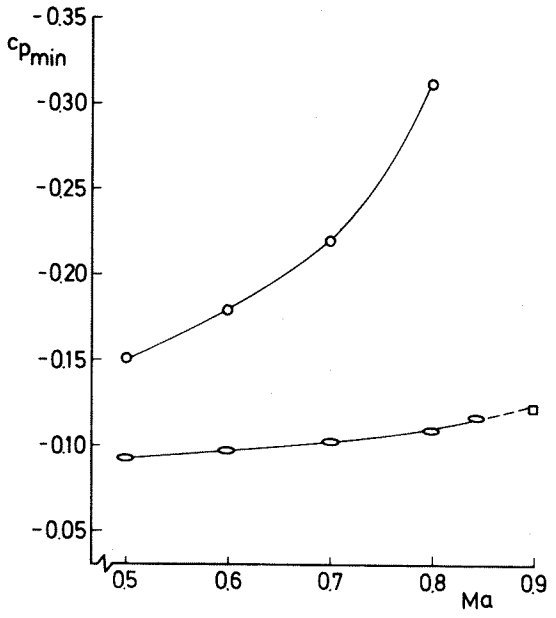

Fig. 11 Minimum c_p values: o not adapted
o adapted wall
□ theory FFA

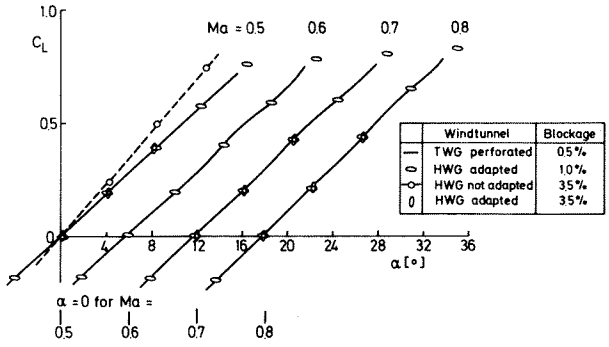

Fig. 14 C_L (α) for AGARD-calibration models

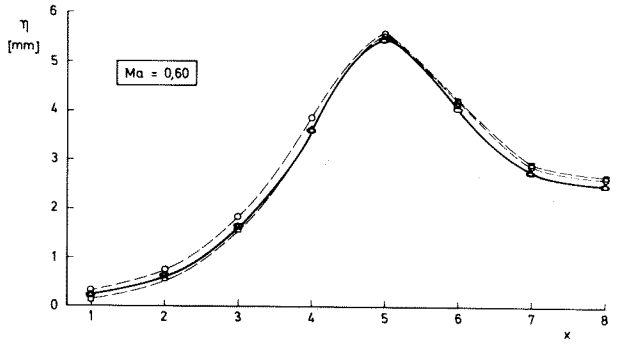

Fig. 12 Adapted wall contour for FFA model
□ = 1. Iteration o = 2. Iteration
△ = 3. " o = 4. "

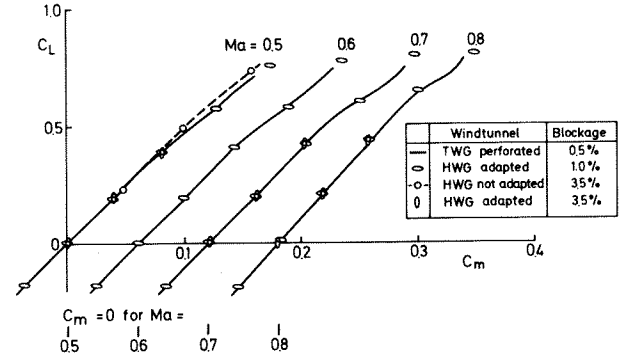

Fig. 15 C_L (C_m) for AGARD-calibration models

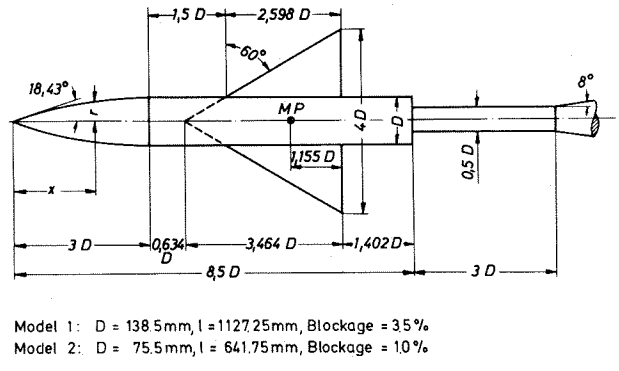

Model 1: D = 138.5mm, l = 1127.25mm, Blockage = 3.5 %
Model 2: D = 75.5mm, l = 641.75mm, Blockage = 1.0 %

Fig. 13 AGARD-calibration model B

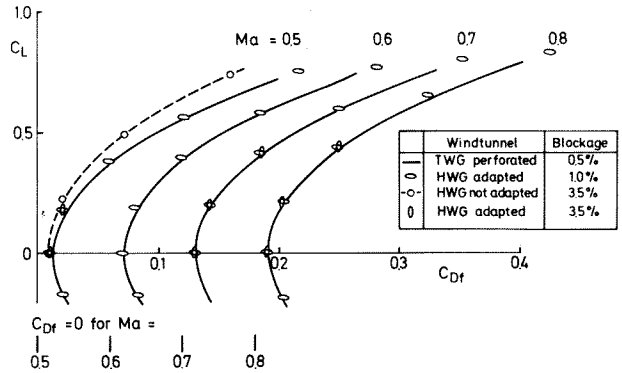

Fig. 16 C_L (C_{Df}) for AGARD-calibration models

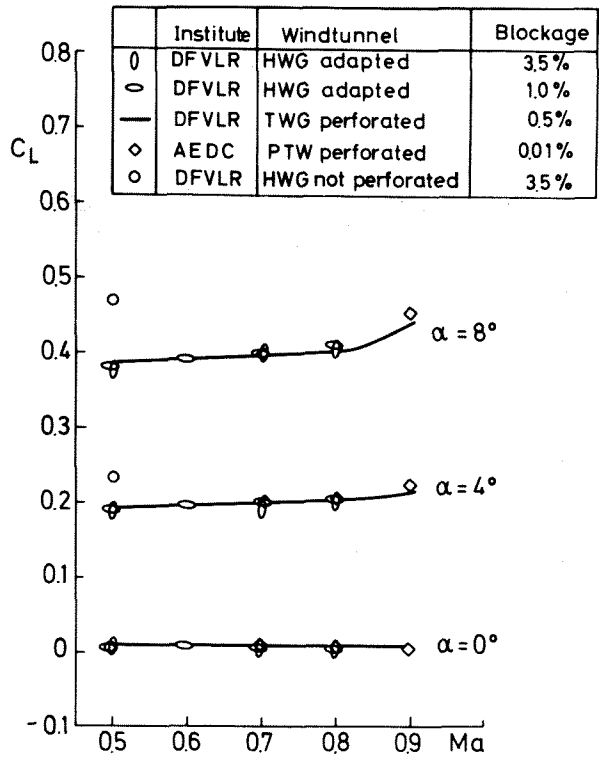

Fig. 17 C_L (Ma) for AGARD-calibration models

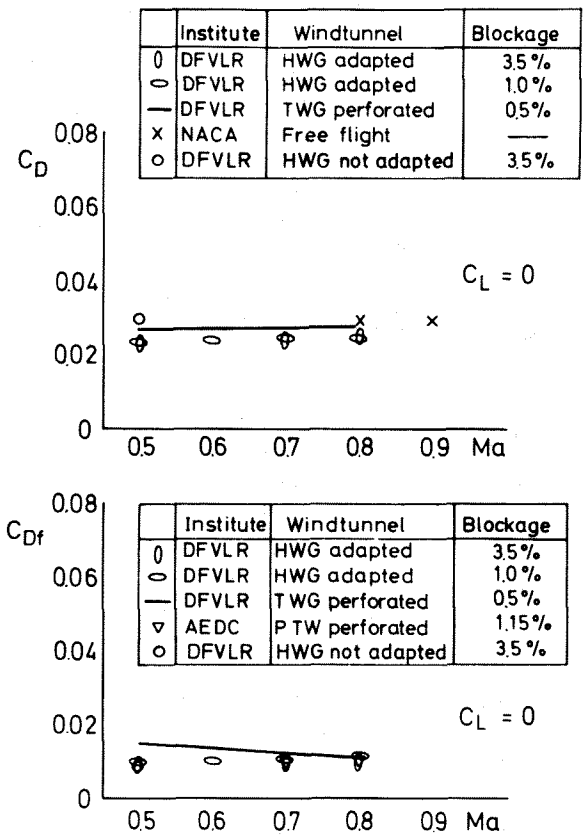

Fig. 19 C_D (Ma) and C_{Df} (Ma) for AGARD-calibration models

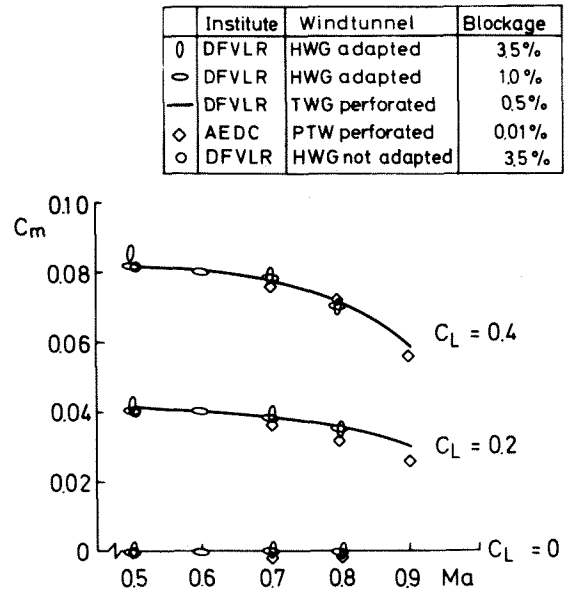

Fig. 18 C_m (Ma) for AGARD-calibration models

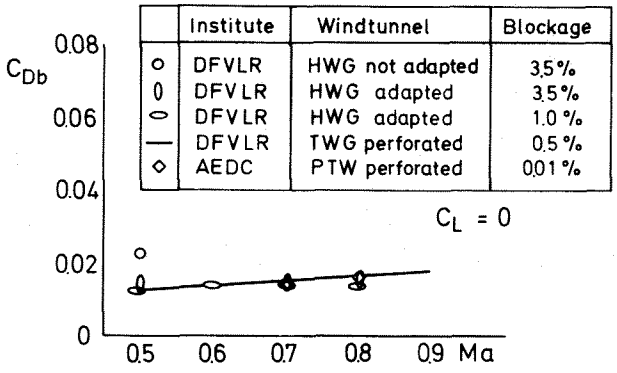

Fig. 20 C_{Db} (Ma) for AGARD-calibration models